High-field multifrequency electron-spin-resonance study of the Haldane magnet $Ni(C_5H_{14}N_2)_2N_3(PF_6)$

T. Kashiwagi,[1] M. Hagiwara,[1] S. Kimura,[1] Z. Honda,[2] H. Miyazaki,[3] I. Harada,[3] and K. Kindo[4]
[1]*KYOKUGEN (Center for Quantum Science and Technology under Extreme Conditions), Osaka University, 1-3 Machikaneyama Toyonaka, Osaka 560-8531, Japan*
[2]*Graduate School of Science and Engineering, Saitama University, 255 Simookubo Saitama, Saitama 338-8570, Japan*
[3]*Department of Physics, Okayama University, 3-1-1 Tsushima-naka, Okayama 700-8530, Japan*
[4]*Institute for Solid State Physics, University of Tokyo, 5-1-5 Kashiwanoha Kashiwa, Chiba 277-8581, Japan*
(Received 19 September 2008; revised manuscript received 2 December 2008; published 6 January 2009)

In order to understand physical properties of the field-induced phase of a spin-gap system, we performed high-field and multifrequency electron-spin-resonance (ESR) measurements on single crystals of the $S=1$ quasi-one-dimensional Heisenberg antiferromagnet, namely, the Haldane magnet, $Ni(C_5H_{14}N_2)_2N_3(PF_6)$, abbreviated as NDMAP. This compound has an energy gap (Haldane gap) at zero field and one of the excited triplet branches goes down on applying magnetic fields, resulting in the gap closing at a critical field H_c around 5 T that is slightly different depending on the field direction. First, we studied the angular dependence of spin excitations below 14 T. Two sets of resonance modes caused by two types of Ni^{2+} chains in NDMAP are observed. These data are analyzed by comparing with a phenomenological field theory (PFT). The experimental results between H_c and about 12 T are well fitted with the calculated ones by the PFT, but the fitting above 12 T is not satisfactory. Therefore, we studied spin excitations at much higher magnetic fields up to about 55 T. Several ESR signals are observed above H_c for each crystallographic axis, and one or two of them survive in the high-field region above about 15 T. One mode approaches a paramagnetic resonance line at high fields and the other mode broadly changes with magnetic fields. These modes fit well with the conventional antiferromagnetic resonance modes with biaxial anisotropy. This result suggests that the quantum fluctuations are suppressed by strong magnetic field and the spin excitations change from a quantum nature to a classical one in high magnetic fields.

DOI: 10.1103/PhysRevB.79.024403 PACS number(s): 76.50.+g

I. INTRODUCTION

Quantum spin systems defined as low dimensional [one-dimensional (1D) or two-dimensional (2D)] antiferromagnets with a small spin value have attracted a number of condensed-matter scientists in the last few decades[1] because they exhibit interesting phenomena, e.g., an energy gap in a one-dimensional antiferromagnet originated from a many-body quantum effect,[2,3] magnetization plateaux due to a quantum origin,[4–7] and high T_c superconductivity.[8–10] Recently, considerable attention has been paid to the field-induced phenomena of the quantum spin-gap systems such as the $S=1/2$ weakly coupled antiferromagnetic dimer,[11–14] the $S=1/2$ antiferromagnetic two-leg spin ladder,[15] the $S=1$ bond-alternating 1D antiferromagnet,[16–18] and the $S=1$ 1D Heisenberg antiferromagnet (HAF), namely, the Haldane magnet.[19]

In these spin-gap systems, the ground state is a singlet and the first-excited one is a triplet at zero magnetic field. The energy of one of the triplet branches decreases with increasing magnetic fields, and the singlet-triplet gap closes at a critical magnetic field H_c which corresponds to a quantum phase-transition point. Interesting physical behavior is expected in the field-induced phase above H_c. For example, in $TlCuCl_3$ which is one of the $S=1/2$ weakly coupled antiferromagnetic dimer systems[11–14] and in $(CH_3)_2CHNH_3CuCl_3$, abbreviated as IPA-$CuCl_3$,[20] which is regarded as the $S=1/2$ two-leg spin ladder,[15] the long-range order (LRO) appeared above H_c at low temperatures is interpreted as a Bose-Einstein condensation (BEC) of magnons.[12] The $S=1$ 1D HAF is expected to show Tomonaga-Luttinger liquid behavior above H_c when the system has an axial symmetry in a magnetic field.[21] Thus, physics in the field-induced phase is one of the interesting topics in recent studies on quantum spin systems, and the low-energy physics near H_c has been studied extensively. Elementary excitations between H_c and H_s, where H_s is the saturation field, have not been clearly understood neither theoretically nor experimentally.

Recently, spin excitations of $TlCuCl_3$ well above H_c were reported, and the spin excitation modes near H_c survive in very high magnetic fields.[22] It is known that these spin excitations are expressed by using a bond-operator model in which the ground state is described by a linear combination of a singlet and a triplet.[23] We are interested in physical properties above H_c of another spin-gap system, namely, the $S=1$ 1D HAF, and the purpose of this study is to make clear the difference in physical properties between these two systems. $Ni(C_5H_{14}N_2)_2N_3(PF_6)$, abbreviated as NDMAP, is one of the $S=1$ quasi-1D HAF compounds and this compound shows the field-induced LRO above H_c at low temperatures. Hence, this Haldane magnet is suitable for the study of the field-induced phase above H_c.

The present paper is organized as follows. In Secs. II and III, physical properties of NDMAP and our experimental apparatus are introduced. Then, we describe the experimental results of electron-spin-resonance (ESR) measurements, followed by the analyses of the results and discussion. Section VI is devoted to conclusions.

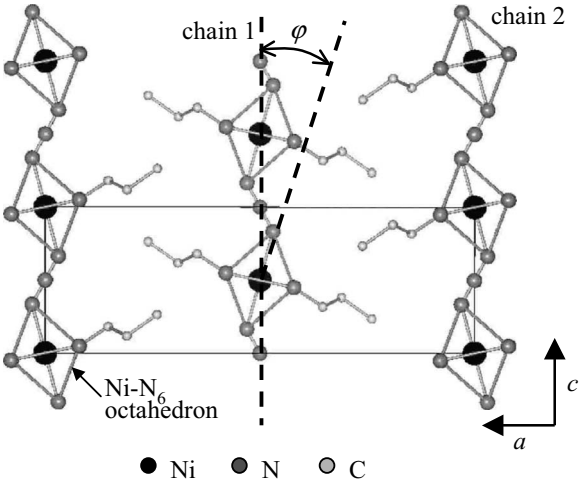

FIG. 1. Crystal structure of NDMAP. There are two types of chains denoted as chain 1 and chain 2.

II. PHYSICS

Single crystals of NDMAP were synthesized according to the method reported by Monfort *et al.*[24] Figure 1 shows a cut view of the crystal structure of NDMAP at 293 K.[25] This compound crystallizes in the orthorhombic system (space group *Pnmn*) with lattice parameters $a=18.046$ Å, $b=8.705$ Å, and $c=6.139$ Å at 293 K. The Ni^{2+} ions are bridged by azido ions forming chains along the c axis and the chains are well separated by PF_6^- anions. The Ni^{2+} ions are surrounded by nitrogen atoms and the principal axis of Ni-N_6 octahedron is tilted from the c axis by $\varphi=16°$ toward the a axis. It is important to note that $H\|c$ is not an axisymmetric field configuration for NDMAP. In addition, there are two types of chains, denoted as chain 1 and chain 2 as shown in Fig. 1, and the tilt direction changes chain by chain. The Ni sites in the chain, however, are crystallographically equivalent, so that no staggered component of the magnetic moments is retained.

The temperature dependence of magnetic susceptibilities of NDMAP was reported and a broad maximum was observed around 40 K for the field directions parallel and perpendicular to the chain.[19] Below 40 K, the susceptibilities decrease steeply toward zero. These are characteristics of a low-dimensional antiferromagnet with a spin gap above a singlet ground state. The susceptibility data are analyzed by using the spin Hamiltonian for the $S=1$ 1D HAF expressed as

$$\mathcal{H} = J\sum_i \boldsymbol{S}_i \cdot \boldsymbol{S}_{i+1} + D\sum_i (S_i^z)^2 - \mu_B \sum_i \boldsymbol{S}_i \cdot \tilde{g} \cdot \boldsymbol{H}, \qquad (1)$$

where J is the nearest-neighbor exchange constant along the chain, $\boldsymbol{S}_i$ the $S=1$ spin operator at the ith site, D the single-ion anisotropy constant, μ_B the Bohr magneton, $\tilde{g}$ the g tensor, and $\boldsymbol{H}$ the external magnetic field. The following parameters were obtained by the fitting $J/k_B=30.0$ K, $D/J=0.3$, $g_\parallel=2.10$, $g_\perp=2.17$, where $g_\parallel$ and $g_\perp$ are the g values parallel and perpendicular to the chain, respectively.[19]

The temperature dependence of the heat capacity (C_p) of NDMAP was measured in applied magnetic fields.[19] No anomaly in C_P was observed in zero magnetic field down to 0.6 K. With increasing fields, a sharp anomaly was observed above H_c and the position of the anomaly does not depend largely on H for $H\|$chain ($H\|c$) but that moves to high-temperature side for $H\perp$ chain ($H\perp c$). The positions of the anomaly are plotted on the magnetic field vs temperature (H-T) plane as shown in Fig. 2. The sharp anomaly of the heat capacity usually indicates the LRO. Thus, this compound shows the phase transition at a field H_{LRO} that depends on the temperature and the direction of external magnetic field. The value of H_{LRO} at $T=0$ corresponds to the critical field H_c and the spin-gap between the ground state and the first-excited states closes at H_c. The low-T and low-H regions below the boundary indicate the Haldane disordered phase, and the region above the boundary represents the LRO phase in its respective field direction. When H is applied parallel to the c axis, an XY symmetry is nearly retained, but for H perpendicular to the c axis, an XY symmetry is broken and an Ising anisotropy is produced. It is known that the phase-transition temperature of an Ising system is higher than that of an XY system for a given space dimensionality. Therefore the boundary of the LRO phase depends on the direction of the external magnetic field. It was mentioned that the change in entropy at the phase boundary is only about 1% of the total entropy expected for the $S=1$ spin system, indicating that the large quantum fluctuations remain in the field-induced long-range ordered phase.[26]

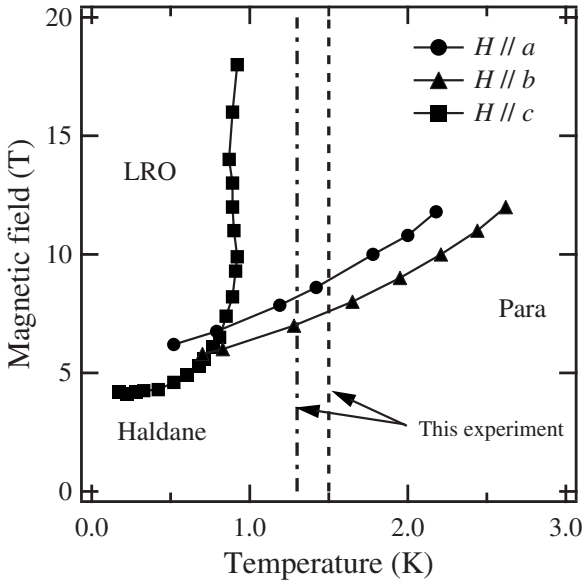

FIG. 2. Magnetic field-temperature (H-T) phase diagram of NDMAP (Ref. 19). The vertical lines at 1.3 and 1.5 K represent the temperatures of the pulse and the static field ESR measurements, respectively.

The heat-capacity measurements in magnetic fields up to 32 T and at temperatures down to 150 mK were performed by Tsujii *et al.*[27] They estimated that the H_c is about 4 T for $H\|c$ and about 6 T for $H\|a$. In addition, they observed an anomaly around 14 T only for $H\|c$. They speculated that this anomaly is a kind of spin rotation around the direction of the applied field parallel to the spin chain.

Chen *et al.*[28] reported the results of elastic neutron-scattering experiments of NDMAP. A striking result of their work is that for a magnetic field applied perpendicular to the chain axis, the high-field phase is no longer a three-dimensional (3D)-ordered state, but it has predominantly the two-dimensional spin correlations. Scans perpendicular to the *bc* plane reveal that the scattering intensity is concentrated in Bragg *rods* along the [1, 0, 0] direction, rather than Bragg *peaks*. The rod nature of the magnetic scattering implies that static spin correlations along the *a* axis are absent in the system and that magnetic ordering occurs only within individual *bc* planes. From this neutron experiment, we obtain new information above H_c. When the magnetic field is applied along the *c* axis, this compound is driven into the 3D LRO. On the other hand, when the magnetic field is applied along the *a* axis, the correlation along the *a* axis does not well grow and the system exhibits a 2D short-range order (SRO).

Inelastic neutron-scattering (INS) experiments at zero and nonzero magnetic fields were performed by Zheludev and co-workers[29,30] and the intrachain exchange constant was determined to be $J=2.6$ meV. Exchange coupling along the *b* axis is considerably weak ($J_b/J \approx 10^{-3}$) and that along the *a* axis is very weak and undetectable ($|J_a/J| < 10^{-4}$). Magnetic anisotropy in NDMAP is predominantly of single-ion easy-plane type with $D/J \approx 0.25$. These values are very similar to those of the analytical results of the magnetic susceptibility. In addition, there is a weak in-plane anisotropy term $E(S_x^2 - S_y^2)$. As a result of these anisotropy effects, the degeneracy of the Haldane triplet is fully lifted at zero field and the gap energies are evaluated as $\Delta_1 = 0.42(3)$ meV, $\Delta_2 = 0.52(6)$ meV, and $\Delta_3 = 1.9(1)$ meV. Correspondingly, the critical fields are strongly dependent on the field orientations.[29,30]

Figure 3 shows the frequency versus field diagrams of the ESR resonance fields at 1.5 K and the INS peaks at 30 mK and some calculated results for (a) $H \| a$ and (b) $H \| c$. The solid circles and the open squares are experimental data of the ESR and the INS, respectively.[29–31] The vertical dotted-dashed lines indicate H_c and the hatching area above H_c corresponds to the field-induced phase. The vertical dashed line for $H \| a$ corresponds to the anomaly of the heat capacity at 1.5 K. Figure 3 clearly shows the Zeeman split of the triplet branches below H_c and reopening the gap above H_c. Below H_c, the triplet was observed by the INS experiments. The ESR branch below H_c is attributed to the transition within the lowest two branches of the triplet. One mode of the triplet reaches the ground state at H_c and the gap reopens above H_c. Then, three modes are observed above H_c for $H \| a$ and $H \| c$ except the lowest ESR mode for $H \| c$. NDMAP does not drive into the LRO phase for $H \| c$ at 1.5 K, but it drives into the LRO phase at about $\mu_0 H_{\mathrm{LRO}} = 9$ T for $H \| a$ as shown in Fig. 2. We stress that the ESR resonance mode for $H \| a$ does not show any anomaly around H_{LRO}.

In the LRO state or well-developed SRO state, the spin excitations can be treated in terms of a spin-wave approximation and only two excitation modes for two sublattice antiferromagnets are defined. This compound shows the LRO with a collinear spin structure above H_c at low temperatures,[28] but we cannot explain the excitation modes

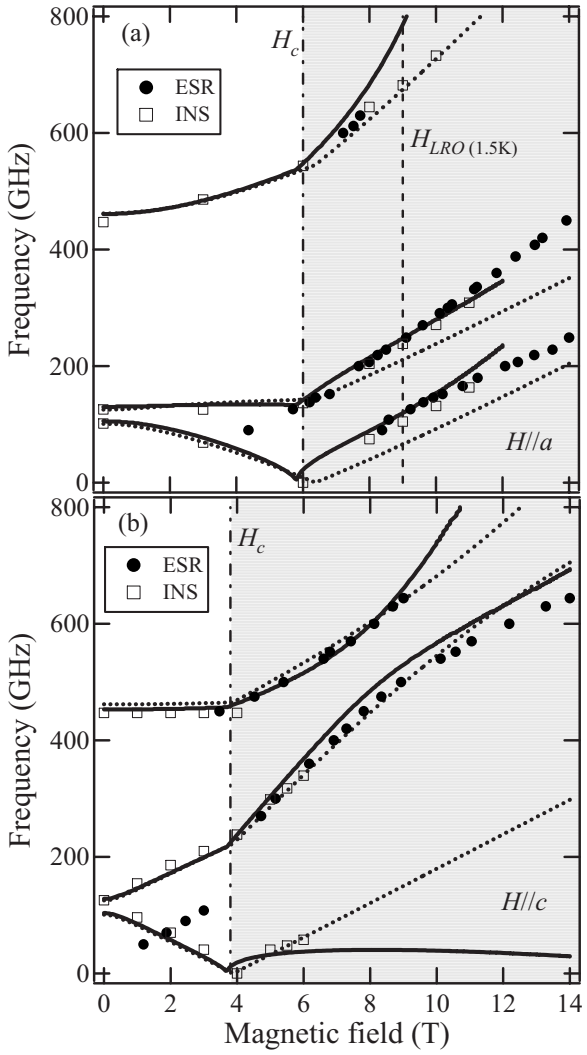

FIG. 3. Frequency versus field diagrams of spin excitations observed by the INS (Ref. 29) and the ESR (Ref. 31) and theoretical curves for (a) $H \| a$ and (b) $H \| c$. The solid circles and the open squares indicate experimental data of the ESR and the INS, respectively. The solid lines and the dotted lines show the results of a PFT reported by Ref. 33 and calculated data of a simple singlet-triplet model assuming the extrapolation of excitation modes below H_c.

above H_c by the conventional spin-wave theory. These spin excitation modes are similar to those observed in the weakly coupled antiferromagnetic dimer $TlCuCl_3$ and the $S=1/2$ antiferromagnetic two-leg spin ladder IPA-$CuCl_3$. The spin excitation modes in NDMAP are calculated by using a phenomenological field theory (PFT) reported by Kolezhuk[32] and obtained good agreement between the experiment and the theory[29,31] near H_c. The anisotropic part of PFT is further modified by Miyazaki *et al.*[33] to treat a spin-reorientation transition at high fields. In Figs. 3(a) and 3(b), the solid and dotted lines show the results of PFT (Ref. 33) and a calculation of a simple singlet-triplet model, respectively. In the latter case, we assume that the excitation modes arise from the branches extrapolated from the singlet and the triplet below H_c. In Figs. 3(a) and 3(b), both calculations show considerably good agreement with experiments near H_c. It is interesting that the naive singlet-triplet model roughly repro-

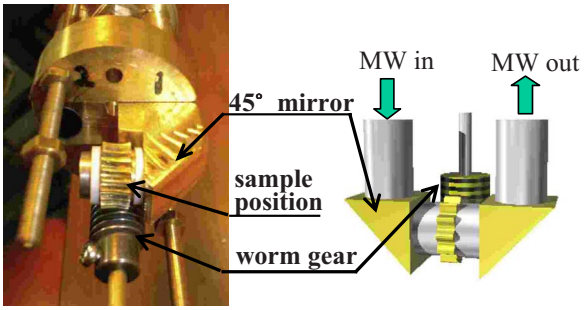

FIG. 4. (Color online) Photograph of probe head of the cryostat for sample rotation and image of the microwave path and the sample rotator.

duces the experimental result near H_c. The disagreement of spin excitations between the calculations and the experiment becomes large at high magnetic fields. This result suggests that the origin of the spin excitations above H_c in NDMAP must be changed by the magnetic field. Therefore, in order to understand the details of physical properties above H_c, we have performed multifrequency and high-field ESR measurements beyond the frequency-field range reported so far on single crystals of the $S=1$ quasi-1D HAF compound NDMAP.

III. EXPERIMENTAL SETUP

We have used two types of ESR measurement systems for this study. The choice of the measurement system depends on the range of the frequency and the magnetic field. One of the ESR measurement systems is composed of a vector network analyzer and a superconducting magnet which covers the frequency up to 700 GHz and the magnetic field up to 16 T. Above this frequency and field range, another ESR measurement system, which is composed of a pulse magnet and microwave sources such as a FIR laser and Gunn and backward oscillators, was utilized.

A. Static field ESR setup

The magnetic field can be swept up to 14 T at 4.2 K and up to 16 T at 2.2 K with a superconducting magnet (Oxford Instruments, UK). An insert [variable-temperature insert (VTI)] is used to change the temperature of the sample space from 1.5 to 300 K. The temperature of the sample is measured by using a calibrated cernox resister thermometer placed close to the sample and is controlled by a heater of Manganin wire. We use a vector network analyzer (MVNA-8–350, AB Millimeter, France) with high-frequency ESA-1 and ESA-2 extensions. Microwaves are introduced into the sample with a cryostat which is made of light pipes with the diameter of 8 mm. A thin stainless-steel jacket is used to avoid the noise from a bubbling of liquid helium. The microwaves for the frequency from about 30 to about 700 GHz can be generated almost continuously.

Figure 4 shows the probe head of the cryostat for sample rotation in magnetic fields. The sample is rotated by using a worm gear and we can change the angle between a crystallographic axis and the direction of the external magnetic field. The microwaves transmit from one side to another side by using two 45° mirrors. This cryostat can be used for all frequency range as mentioned above. Usually, a sample is put on a brass sample holder and fixed with vacuum grease or a silver paste. Since the sample holder has a hole, we can detect the microwave through the sample. This cryostat enables us to measure the angular dependence of spin excitations of a target compound at frequencies up to about 700 GHz.

B. Pulsed-field ESR setup

Submillimeter waves at a frequency from about 500 GHz to about 7 THz are generated with a FIR laser and those at the frequency below 500 GHz are obtained by using several Gunn oscillators and backward wave oscillators (BWOs). A pulsed magnet can generate magnetic fields up to about 55 T with the duration time of about 7 ms.[34] The magnetic field is measured as the time derivative of magnetic field with a field pickup coil. The magnitude of the magnetic field is obtained by integrating the curve of dH/dt. ESR measurements at low temperatures down to 1.3 K were performed by pumping liquid ^{4}He. As well as the static field ESR system, microwaves are introduced to the sample via light pipes with the diameter of 4 mm and a thin stainless-steel jacket is used because of the same reason as before. ESR signals are detected with an InSb hot-electron bolometer (QMC Instruments Ltd.).

IV. EXPERIMENTAL RESULTS

First, we show the experimental results of ESR measurements near H_c region. Then we describe the results of high magnetic field region ($H \gg H_c$). As mentioned above, the experimental results near H_c were obtained by utilizing the static field ESR measurement system and the data in high magnetic fields were taken by using the pulsed-field ESR measurement system.

A. Spin excitations near H_c region

As mentioned in Sec. II, there are two types of Ni^{2+} chains in which each tilt direction of the principal axis of Ni-N_6 octahedron is different. In Figs. 5(a) and 5(b), the relation between the crystallographic axes, the principal axes of Ni-N_6 octahedron, and the external magnetic field (H) are shown. The z_1 and z_2 directions represent one of the principal axes of Ni-N_6 octahedron in two kinds of chains and φ shows an angle between the c axis and the $z_1(z_2)$ axis and is about 16°. The θ is an angle between the c axis and the direction of the external magnetic field in the ac plane, and the $\theta_1(\theta_2)$ shows the angle between the $z_1(z_2)$ axis and the direction of the external magnetic field. The ψ in Fig. 5(b) is an angle between the a axis and the direction of the external magnetic field in the ab plane.

The frequency-field dependence of spin excitations below 14 T for $H \| a$ and $H \| c$ was reported in Ref. 31. Thus, we investigate angular dependences of these spin excitations to get additional information on spin excitations above H_c and to clear the relationship between the spin excitations and the

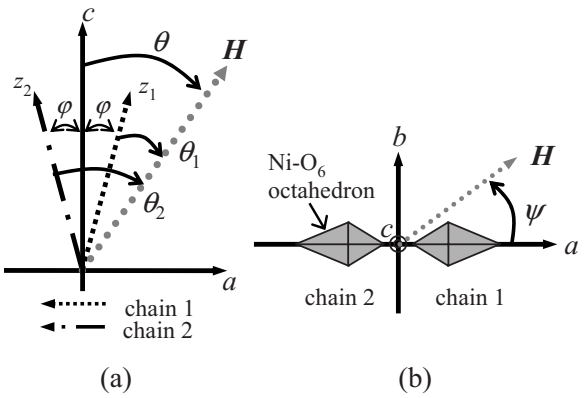

FIG. 5. Relation between the crystallographic axes and the external magnetic field in (a) the *ac* plane and (b) the *ab* plane.

crystal structure. From the neutron-scattering experiments, it was reported that the two types of chains in NDMAP behave independently against the external magnetic field.[35] In addition, Ref. 33 showed an interesting $H-\theta_i$ $(i=1,2)$ phase diagram of the sublattice magnetization at zero temperature, where the θ_i stands for the angle between the external magnetic field and one of the principal axes of Ni-O_6 octahedron in the two types of chains. According to that study, a spin-flop-like transition was expected for $\theta_i \sim 0.1\pi$.[33]

The angular θ dependence of the ESR spectra was measured at four different frequencies of 200.0, 300.0, 404.1, and 505.1 GHz, and the angular ψ dependence was measured at 200.3 and 300.4 GHz. Here, we only show the results of 200.0 and 505.1 GHz for the θ dependence. Figures 6 and 7 display the typical angular θ and ψ dependences of the ESR spectra of NDMAP.

Figure 6(a) shows the angular θ dependence of ESR spectra at 200.0 GHz in the *ac* plane. There are two sets of angular dependent ESR signals reflecting the two kinds of chains in NDMAP. The signals for one set are denoted as α_1 and β_1 and those for another set are denoted as α_2 and β_2. The principal axis of the α_1 or α_2 signal is deviated by about 20° from the *a* axis, which is the same as that for the principal axis of the β_1 or β_2 signal. The signal of α_1 near the *c* axis is very weak. At 300.0 GHz, similar angular dependence to that at 200.0 GHz was observed. Angular dependent ESR signals for two sets denoted $\alpha_1(\alpha_2)$ and $\beta_1(\beta_2)$, corresponding to the same notation signals at 200 GHz, shift to the high-field sides. At 404.1 GHz, we only observed the angular dependent ESR signals $\alpha_1(\alpha_2)$. The signals denoted $\beta_1(\beta_2)$ must be out of the measurement range. Figure 6(b) shows the angular θ dependence of ESR spectra at 505.1 GHz in the *ac* plane. The results at 505.1 GHz are very similar to those at 404.1 GHz except observing new signals denoted as γ around 6 T which is insensitive to the magnetic field direction. The signals of α_1 and α_2 are clearly observed at most of the angles. These results suggest that the signal intensity becomes strong with increasing magnetic fields and frequency.

The existence of the angular dependent signals symmetric to the *a* axis suggests that each different kind of chain in NDMAP behaves independently against the external magnetic field, which is consistent with the results of the INS experiment.[35] This independent behavior of the two kinds of chains is very interesting because the signals around the *a* axis were observed in the LRO phase at 1.5 K, which means that cooperative behavior is expected.

The angular ψ dependence of ESR spectra at 200.3 GHz in the *ab* plane is shown in Fig. 7(a). The angular ψ dependent signals denoted as ξ and the nearly angular independent signals denoted as η were observed. In the *ab*-plane rotation, we did not observe the signal sets symmetric to the *a* or *b* axis like in the *ac*-plane angular dependence. The separation of the signals ξ near the *a* axis must be caused by the inadequate sample setting. Figure 7(b) displays the angular ψ dependence of the ESR spectra at 300.4 GHz in the *ab* plane. Another mode denoted as ζ is visible in this figure. The intensity of the signals ζ is weaker than those of the signals ξ and η. The separation of the signals η near the *a* axis must be caused by the same reason as observed at 200.3 GHz. Since the two types of chains in NDMAP are equivalent against the external magnetic field in this rotation, we expect

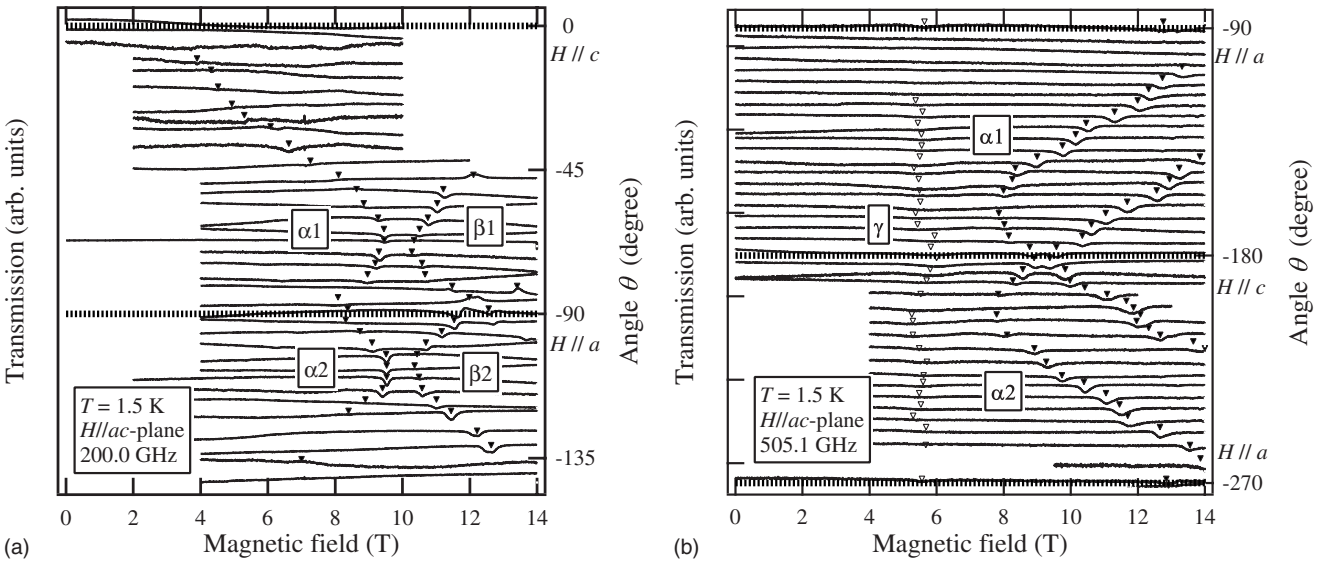

FIG. 6. Angular θ dependence of ESR spectra at (a) 200.0 GHz and (b) 505.1 GHz at 1.5 K.

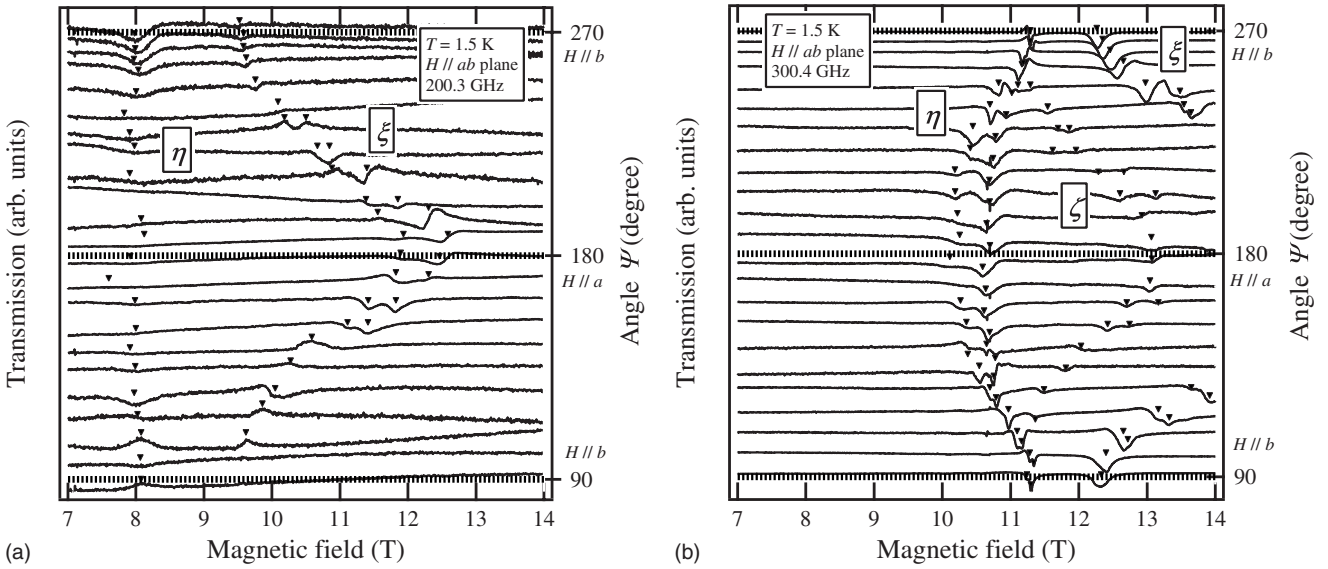

FIG. 7. Angular ψ dependence of ESR spectra at (a) 200.3 GHz and (b) 300.4 GHz at 1.5 K.

no separation of the signals in the angular ψ dependence. The resonance fields in the θ versus H and the ψ versus H planes are shown in Figs. 8 and 9, respectively.

B. Spin excitations in very high magnetic fields from H_c

The spin excitations in high magnetic fields up to about 50 T for $H\|a$ and $H\|c$ were reported.[36] In this section, we show the ESR spectra in high magnetic fields up to about 50 T for $H\|b$ and compare the results of the spin excitations for different crystallographic axes. The configuration of $H\|b$ corresponds to another $H\perp$ chain configuration. The typical ESR spectra are shown in Figs. 10(a) and 10(b). The magnetic field was corrected by the ESR standard signal ($g=2.0036$) of diphenyl-picrylhydrazyl (DPPH). Figure 10(a) shows the ESR spectra below about 500 GHz and two strong signals are denoted as B-1 and B-4. The B-4 signal is broaden with increasing frequency. Similar behavior of the signal near 400 GHz was found for $H\|a$ (not shown). The ESR spectra above about 500 GHz are shown in Fig. 10(b) and three signals are denoted as B-1, B-2, and B-3. The intensity of the signal B-1 is stronger than those of the signals B-2 and B-3. The linewidth of the B-1 signal becomes large above about 1000 GHz. Similar behavior was observed in the ESR spectra for $H\|c$, but we see the change in the linewidth more clearly for $H\|b$. The frequency versus field diagrams of ESR resonance fields for three crystallographic axes are shown in Figs. 11(a)–11(c). The data indicated by the filled triangles for $H\|a$ and $H\|c$ below 14 T are taken from previous experiments in a steady field at 1.5 K reported by Hagiwara *et al.*[31] The open diamond symbols in Figs. 11(a) and 11(c) are the results of the INS experiments reported by Zheludev *et al.*[29] The large and small signals are indicated by filled and open symbols, respectively. The strong signal for each axis approaches to each paramagnetic resonance line with increasing magnetic fields. The slopes of

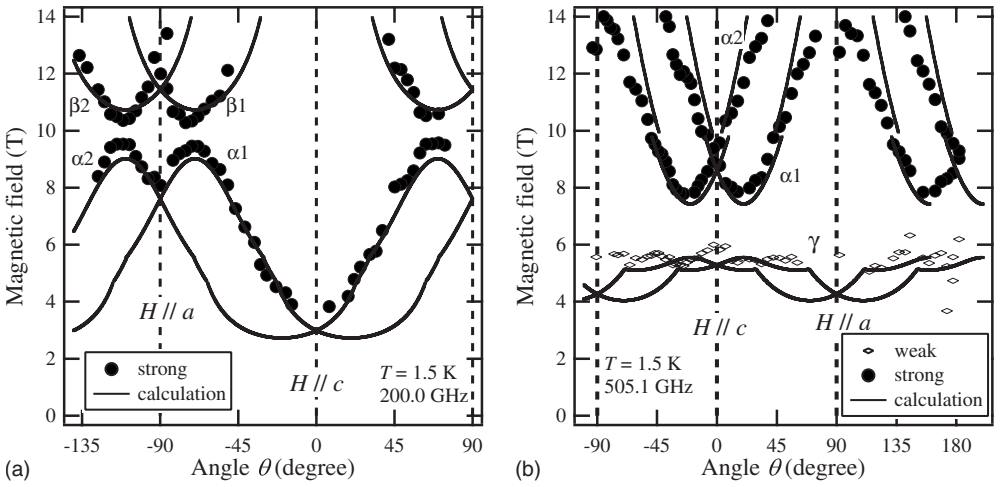

FIG. 8. Angular θ dependence of ESR resonance fields at (a) 200.0 GHz and (b) 505.1 GHz. Solid lines show the results of the PFT calculations.

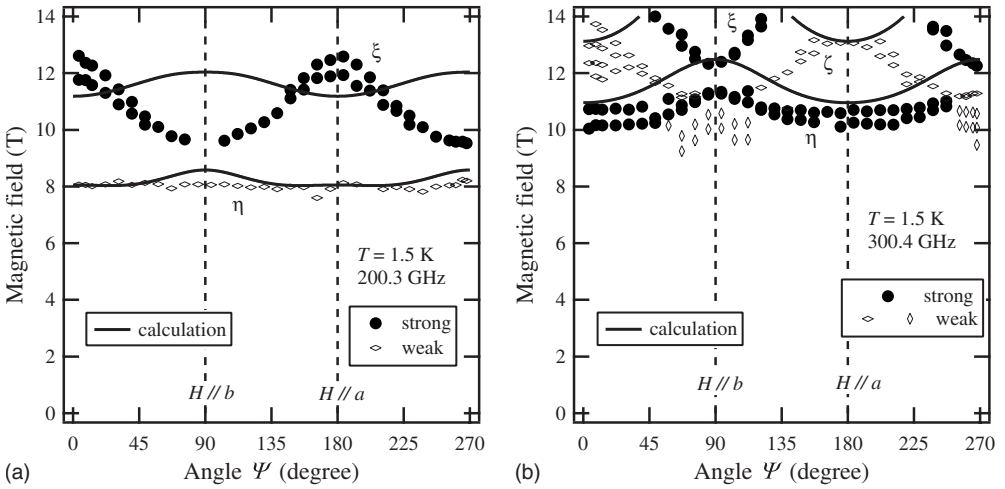

FIG. 9. Angular ψ dependence of ESR resonance fields at (a) 200.3 GHz and (b) 300.4 GHz. Solid lines show the results of the PFT calculations.

the A-2, B-2, and C-2 branches are nearly twice of the g value of each axis and these signals disappear at about 15 T. The behavior of the A-4 signal is similar to that of the B-4 signal. Since we do not have any good submillimeter-wave sources operating at around 500 GHz for the pulsed-field ESR experiment, the connection between the modes A-5 and A-1 or A-3 is not clear.

V. ANALYSIS AND DISCUSSION

We apply two theoretical methods to analyze the experimental results of spin excitations in NDMAP. First, we analyze the spin excitations observed in a magnetic field below 14 T by using a PFT. It is known that the PFT explains well the experimental INS results in NDMAP near H_c. Then, we analyze the experimental data observed in high magnetic fields above about 15 T by using a conventional antiferromagnetic resonance (AFMR) theory because quantum fluctuations are expected to be suppressed by strong magnetic fields.

A. Analysis of spin excitations near H_c

It was reported that the PFT calculations done by Kolezhuk and co-workers[29,31] reproduce well the INS and the ESR experimental results of NDMAP. Recently, the PFT calculations were modified by Miyazaki *et al.*[33] They carefully treated the anisotropy in higher order terms and obtained a Lagrangian as follows:

$$\mathcal{L} = \sum_{i=x,y,z} \left\{ \frac{1}{\tilde{m}_i}[(\partial_t \phi_i)^2 - v_i^2(\partial_x \phi_i)^2] - 2\frac{1}{\tilde{m}_i}(\boldsymbol{h} \times \boldsymbol{\phi})_i \partial_t \phi_i - U_2(\boldsymbol{\phi}) - U_4(\boldsymbol{\phi}, \partial_t \boldsymbol{\phi}) \right\}, \quad (2)$$

where $\boldsymbol{\phi}$ is the staggered order parameter, which is related to the sublattice magnetization, $\tilde{m}_i$ is the phenomenological parameters, v is the characteristic velocity, and $\boldsymbol{h}$ is the external magnetic field. The quadratic and quartic parts of the potential are given by

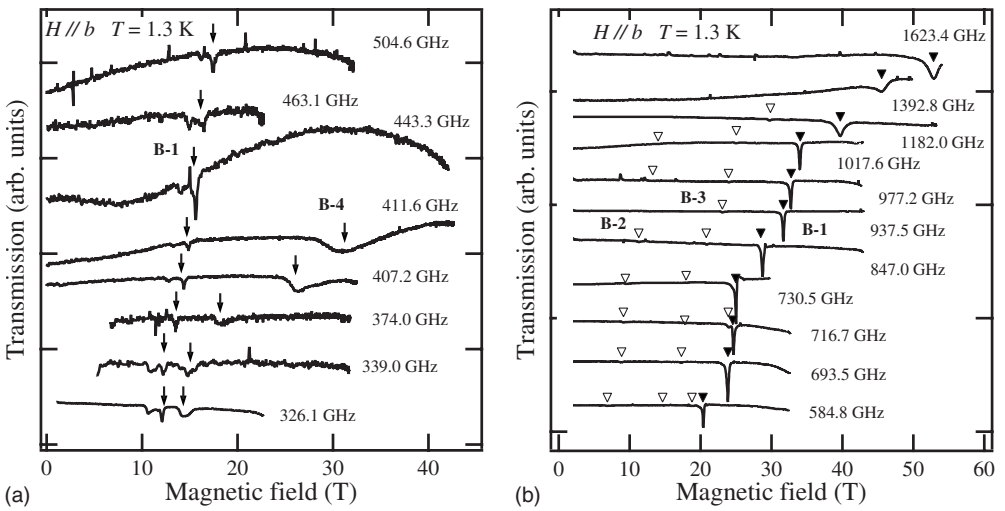

FIG. 10. Frequency dependence of ESR spectra of NDMAP at 1.3 K for $H \| b$ (a) below about 500 GHz and (b) above about 500 GHz.

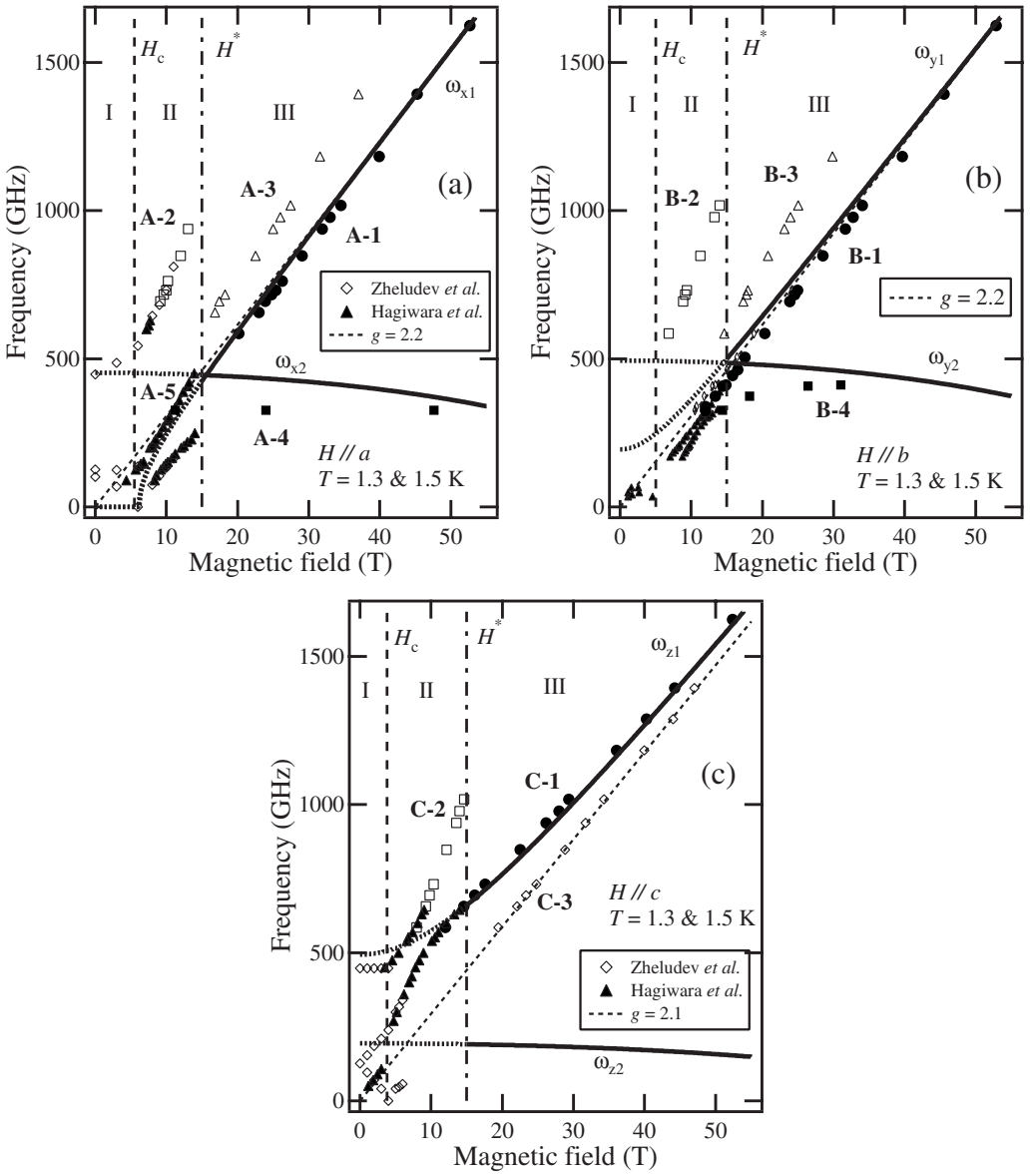

FIG. 11. Frequency versus field diagrams of ESR resonance fields for (a) $H\|a$, (b) $H\|b$, and (c) $H\|c$. Solid and dotted lines represent the conventional AFMR calculations. Vertical broken and dotted-broken lines correspond to H_c and H^*.

$$U_2(\boldsymbol{\phi}) = \sum_i \left[m_i \phi_i^2 - \frac{1}{\tilde{\boldsymbol{m}}_i} (\boldsymbol{h} \times \boldsymbol{\phi})_i^2 \right], \tag{3}$$

$$U_4(\boldsymbol{\phi}, \partial_t \boldsymbol{\phi}) = \sum_i \lambda_i \phi_i^2 \boldsymbol{\phi}^2 + \sum_{i,j} \lambda_{1,ij} \phi_i^2 \frac{1}{\tilde{\boldsymbol{m}}_j^2} F_j^2 + \sum_{ij} \lambda_{2,ij} \frac{\phi_i \phi_j}{\tilde{\boldsymbol{m}}_i \tilde{\boldsymbol{m}}_j} F_i F_j, \tag{4}$$

$$\boldsymbol{F} = -\partial_t \boldsymbol{\phi} + \boldsymbol{h} \times \boldsymbol{\phi}. \tag{5}$$

The modification has been introduced only in U_4 to treat the anisotropy more appropriately. If we set $\lambda_i = \lambda$, $\lambda_{1,ij} = \lambda_1$, and $\lambda_{2,ij} = \lambda_2$, we obtain the quartic potential obtained by Zheludev *et al.*[29] Note here that $\lambda_{2,ij}$ is a symmetric tensor, $\lambda_{2,ij} = \lambda_{2,ji}$.

The transition from the Haldane phase to the ordering phase is triggered by static nonzero solution, $\boldsymbol{\phi}^{(0)}$, where $\boldsymbol{\phi}^{(0)}$ is a solution where the static part of the potential U_2 has a minimum. This transition is characterized by the change in the sign of its second derivatives. Two kinds of transitions, namely, transitions from the Haldane phase to the xz phase and to the y phase, are possible depending on θ which is the angle between the c axis and the direction of external magnetic field. Here, the xz and the y phases are named by the appearance of sublattice magnetization in the xz and the yz planes, respectively.

The excitation energies are obtained by the equation of motion for three small fluctuations around the static solution obtained. If the secular equations are linearized, three excitation modes and their energies are obtained.[33]

The phenomenological parameters m_i, $\tilde{\boldsymbol{m}}_i$, λ_i $(i=1,2,3)$, $\lambda_{1,ij}$, and $\lambda_{2,ij}$, were chosen so that their PFT calculation

reproduce the magnetic field dependence of the excitation energies observed by the INS and the ESR experiments in magnetic fields. Parameter values as well as a detailed discussion on the parameters for PFT can be seen in Ref. 33.

Using the parameter values given in Ref. 33, we analyze the experimental data of the angular dependences of ESR resonance fields below 14 T. Figures 8(a) and 8(b) show the comparison between the experiment and the calculation in the *ac* plane at 200.0 and 505.1 GHz, respectively. It is obviously seen that the experimental results are satisfactorily explained by the PFT calculations.

We notice that the agreement between the experiment and the PFT calculation is not good above 12 T near $H\|a$. One of the reasons of this disagreement may be the applicable magnetic field range of the PFT calculations because the PFT calculations are obtained under an assumption that the magnetic field is not far from H_c. The PFT calculations also predicted the phase transition at a critical angle θ_c,[33] but we could not observe any anomalies around θ_c. This disagreement between the experiment (1.5 K, no LRO) and the calculation (0 K, LRO) must be caused by whether or not the system is ordered.

The comparisons of the angular ψ dependence of the ESR resonance fields in the *ab* plane at 200.3 and 300.4 GHz with that by the PFT calculations are shown in Figs. 9(a) and 9(b). The mode denoted as η at 200.3 GHz is roughly explained by the PFT calculation, but the same mode at 300.4 GHz and the mode denoted as ζ are not reproduced by the calculations. This disagreement may be caused by the phenomenological parameters determined from the fittings of the data for $H\|a$ and $H\|c$.

B. Analysis of spin excitations in high magnetic fields above 15 T

The characteristic excitation modes in Figs. 11(a)–11(c) are roughly divided into three magnetic field regions: I, II, and III. The boundary between I and II is the critical field H_c which is indicated by the broken vertical line, and the boundary between II and III is denoted by H^* which is indicated by the dotted-broken vertical line. Since the energy gap between the singlet and the triplet is open below H_c, we expect to observe ESR signals from the transitions within the triplet states in region I. We observed the ESR signal corresponding to the transition between the lowest two triplet branches. In the field-induced phase above H_c, several resonance modes were observed in region II. In this region, we add some highest mode data up to about 1000 GHz to the previously reported ones. The highest mode has nearly twice the g value of the intrinsic value of Ni^{2+} ion for each direction, and the signal intensities of the modes decay with increasing magnetic fields and disappear around 15 T. The large signals denoted as **A**−**1**, **B**−**1**, and **C**−**1** in Figs. 11(a)–11(c) survive above H^* and approach their paramagnetic lines at high fields. The signal intensities of the modes **A**−**3**, **B**−**3**, and **C**−**3** are very weak. Since we have no submillimeter wave sources around 500 GHz, the connection of modes between regions II and III for $H\|a$ is not clear. But it can be smoothly connected the modes between regions II and III for $H\|b$ and $H\|c$. The mode **C**−**3** might be the signal from an impurity, and this signal must be hidden by the large signal **A**−**1** and **B**−**1** for $H\|a$ and $H\|b$, respectively. The modes **A**−**4** and **B**−**4** were broadly field independent.

An anomaly in specific heat around 14 T was reported,[27] but this anomaly was only observed for $H\|c$. Thus, it is difficult to relate the anomaly of the specific heat to the boundary between regions II and III. Spin-reorientation transition of the field-induced LRO phase was proposed for the origin of this anomaly by Miyazaki *et al.*[33] It should be noted that NDMAP is not driven into the LRO phase at 1.3 or 1.5 K for $H\|c$, but is driven into the LRO (or 2D SRO) phase around 9 T at this temperature for $H\|a$. Therefore, the anomaly observed in the specific-heat measurement for $H\|c$ could not be observed in the ESR measurements.

A spin reduction has been reported in the neutron-scattering experiment in the LRO phase above H_c.[29] Hence, quantum fluctuations, which must be suppressed at high magnetic fields, affect this system even in the LRO phase above H_c. For $H\|c$, the system does not enter the LRO phase at 1.3 K, but a short-range order must be well developed in high magnetic fields. For $H\perp c$, this compound is driven into the LRO or 2D SRO phase at 1.3 K. As described in Sec. II, the field direction changes the symmetry of the system. Usually, quantum fluctuations in a system with Ising symmetry are weaker than those in a system with XY symmetry. Thus, quantum fluctuations must be weak for the $H\perp c$ and it is expected that classical antiferromagnetic behavior appears above H_c, but we found that the ESR modes between H_c and H^* are different from those expected in a classical antiferromagnet. Only two resonance modes are expected for the two sublattice antiferromagnet systems. Therefore, we suppose that a change from a quantum state to a nearly classical one occurs at H^* for each crystallographic axis. Accordingly, we analyze the ESR signals observed at high fields above H^* in terms of conventional AFMR modes. The conventional theory of AFMR for two sublattices is summarized in Ref. 37. NDMAP has an axial single-ion anisotropy $D>0$ and a very small anisotropy in the xy plane. Thus, the AFMR modes with biaxial anisotropy at high magnetic fields above H^* in NDMAP can be expected. The AFMR modes in Ref. 37 are applicable in the low magnetic field region and not at high magnetic fields. Hence, the AFMR modes up to high magnetic fields reported in Refs. 38 and 39 were used in the analyses of the AFMR modes above H^* in NDMAP. The AFMR modes up to the saturation field are given as follows:

(1) $H\|x$ (easy axis) and $H>H_F$ (H_F is a spin-flop field),

$$\left(\frac{\omega_{x1}}{\gamma}\right)^2 = H^2 - C_1, \tag{6}$$

$$\left(\frac{\omega_{x2}}{\gamma}\right)^2 = (C_2 - C_1) - (C_4 - C_3)H^2, \tag{7}$$

(2) $H\|y$ (second easy axis),

$$\left(\frac{\omega_{y1}}{\gamma}\right)^2 = H^2 + C_1, \tag{8}$$

$$\left(\frac{\omega_{y2}}{\gamma}\right)^2 = C_2 - C_4 H^2, \tag{9}$$

(3) $H \| z$ (hard axis),

$$\left(\frac{\omega_{z1}}{\gamma}\right)^2 = H^2 + C_2, \tag{10}$$

$$\left(\frac{\omega_{z2}}{\gamma}\right)^2 = C_1 - C_3 H^2, \tag{11}$$

and

$$C_1 = 2H_{A1}H_{\mathrm{ex}}, \tag{12}$$

$$C_2 = 2H_{A2}H_{\mathrm{ex}}, \tag{13}$$

$$C_3 = \frac{H_{A1}}{2H_{\mathrm{ex}}}, \tag{14}$$

$$C_4 = \frac{H_{A2}}{2H_{\mathrm{ex}}}, \tag{15}$$

where H_{ex} is the exchange field and H_{A1} and H_{A2} the orthorhombic anisotropy fields ($H_{A1} < H_{A2}$). The definitions of these parameters are shown below:

$$\gamma = \frac{g\mu_B}{\hbar}, \tag{16}$$

$$A = \frac{zJ}{(g\mu_B)^2}\left(\frac{2}{N}\right), \tag{17}$$

$$M_0 = \left(\frac{N}{2}\right) g\mu_B S, \tag{18}$$

$$H_{\mathrm{ex}} = AM_0, \tag{19}$$

$$H_{A1} = \frac{K_1}{M_0}, \tag{20}$$

$$H_{A2} = \frac{K_2}{M_0}, \tag{21}$$

where $\hbar$ is Planck's constant divided by 2π, A the molecular-field constant of the two sublattices, N the number of magnetic ions, z the number of neighboring site, and K_1 and K_2 the anisotropy constants for the second easy axis and the hard axis, respectively.

These equations are extracted under the assumption of $H_{\mathrm{ex}} \gg H_{A1}$, H_{A2} which is realized in NDMAP. The resonance modes denoted as ω_{x2}, ω_{y2}, and ω_{z2} show the softening at the saturation magnetic fields $H_s = 2H_{\mathrm{ex}}$. We fitted the experimental data in high magnetic fields by using these AFMR modes and the calculated data are plotted with solid (above H^*) and dotted (below H^*) lines indicated by ω_{x1} and ω_{x2} for $H \| a$, ω_{y1} and ω_{y2} for $H \| b$, and ω_{z1} and ω_{z2} for $H \| c$ in Figs. 11(a)–11(c), respectively. Satisfactory agreement between the experiment and the calculation in the high magnetic field region is obtained. The following parameters are used to calculate the AFMR modes: $\mu_0 H_{\mathrm{ex}} = 41$ T, $\mu_0 H_{A1} = 0.46$ T, and $\mu_0 H_{A2} = 3.08$ T using $S=1$, $J/k_B = 30.5$ K, $g_a = g_b = 2.17$, and $g_c = 2.2$. The parameters, except for H_{A1} and H_{A2}, are very close to the values reported in previous experiments on NDMAP.[19,29,31] It is known that the saturation field of the $S=1$ 1DHAF is $H_s = 4J/(g\mu_B)$. Accordingly, $\mu_0 H_s = 82$ T is estimated with $J/k_B = 30$ K.

The strong signals denoted as **A**−**1**, **B**−**1**, and **C**−**1** approach the paramagnetic resonance lines at high magnetic fields and these are well explained by the AFMR modes denoted as ω_{x1}, ω_{y1}, and ω_{z1}. In addition, the signals **A**−**4** for $H \| a$ and **B**−**4** for $H \| b$ approach the AFMR mode indicated by ω_{x2} and ω_{y2} in high magnetic fields, respectively. Unfortunately, there are no microwave sources in our facility to observe the signals corresponding to the ω_{z2} mode. Consequently, these results suggest that the quantum fluctuations are suppressed and the spin excitations of NDMAP at high fields can be expressed by the conventional AFMR modes.

C. Discussion

To discuss the spin excitations in NDMAP, the experimental results are compared to those of other spin-gap compounds such as $TlCuCl_3$ and IPA-$CuCl_3$. Below H_c, the energy states of these spin-gap materials are described by a similar singlet-triplet picture. The ground state is a singlet and the lowest excited states are a triplet. The triplets are split by magnetic fields and the spin excitations were observed by the INS measurements.[14,15,29] The observed spin excitations show similar behavior between these three compounds except the single-ion type anisotropy effect which comes from the difference of the magnetic ion in these compounds. The magnetic ions in $TlCuCl_3$ and IPA-$CuCl_3$ are Cu^{2+} ions ($S=1/2$), but those in NDMAP are Ni^{2+} ions ($S=1$).

The energy gap between the singlet and the lowest triplet closes at H_c which corresponds to a quantum phase-transition point. At low enough temperatures and above H_c, these compounds exhibit a LRO because of the weak interdimer or interchain interactions. Since large quantum fluctuations are expected in the vicinity of H_c, the low-energy dynamics must be strongly influenced by the longitudinal oscillations of the ordered magnetic moments. This suggests a difference between the dynamics of the field-induced ordered state and that of a conventional antiferromagnet. Therefore, the low-energy dynamics of the field-induced LRO state near H_c cannot be described by the conventional spin-wave formalism, even at $T=0$ K.

The spin excitations in the spin-gap systems were discussed by Kolezhuk and Mikeska[40] in terms of the hardcore boson approximation, and they concluded that the magnetic-field dependence of the triplet excitation energies changes at H_c from $g\mu_B H S_z$ to $g\mu_B H(1-S_z)$, where $S_z = \pm 1, 0$. Thus, two modes have a gap above H_c and the difference of the slope of these modes is twice. For the $S=1$ quasi-one-dimensional antiferromagnet, Affleck[41] studied the spin excitations above H_c for an axial symmetric case and an axial

symmetry-breaking case. In the case of the axial symmetry, two modes were calculated and one mode is gapless and the other one has a gap above H_c. For the axial symmetry-breaking case, two spin excitation modes have a gap above H_c. Hence, we know that anisotropy plays a very important role in the energy states above H_c.

The spin excitations between these compounds in the vicinity of H_c are well explained by the above interpretations. In fact, two spin excitation modes with different slopes which correspond to g and $2g$ of the magnetic ion of each compound were observed above H_c by the INS measurements in these compounds.[13,14,42,43] Accordingly, the existence of the higher-lying spin excitations with the slope of g and $2g$ is one of the common characteristics in the quantum spin-gap systems. The anisotropy affects the lowest excitation mode. In $TlCuCl_3$, the lowest excitation mode has a gap and it was observed by the ESR measurements.[44] The smallest field-induced gap in $TlCuCl_3$ is explained by Dzyaloshinski-Moriya-type anisotropy and magnetoelastic effects.[43] The lowest excitation mode in NDMAP also has a gap that is caused by a low symmetry due to the single-ion anisotropy in this compound. On the other hand, the energy gap of the lowest excitation mode in IPA-$CuCl_3$ was not observed by the INS measurements.[42,43] The observed gapless mode in this compound was interpreted as the Goldstone mode associated with the spontaneous breaking of rotational symmetry due to magnetic ordering,[43] but the small gap may not be observed by the INS measurements because of the low-energy resolution.

As mentioned in Sec. I, the spin excitations observed in $TlCuCl_3$ were analyzed in terms of a bond-operator model which explained well the experimental results in high magnetic fields.[22,23] In this bond-operator model, the ground state is described by a linear combination of the singlet and the triplet, which changes continuously from a pure singlet character at H_c to a pure triplet state at the saturation field. This implies that the number of nearly noninteractive triplet magnons increases with the field above H_c. Then, the excitation mode with a slope of $2g$ was interpreted to be a consequence of the triplet pair-creation process according to the bond-operator model. We suppose that the excitation modes in the vicinity of H_c observed in NDMAP and IPA-$CuCl_3$ arise from a similar origin to that in $TlCuCl_3$ and the difference in excitation modes between these compounds must be caused by the alteration of interactions among the magnons with increasing magnetic fields.

Two higher-lying excitation modes with slopes of g and $2g$ show different behaviors between these compounds with increasing magnetic fields. The spin excitations in $TlCuCl_3$ in magnetic fields up to about 50 T were reported. These two gapped modes are robust against magnetic fields[22] and are different from excitation modes in a conventional antiferromagnet. This reflects the effect of strong coupling in the antiferromagnetic dimers. On the other hand, in NDMAP, the $2g$ excitation modes denoted as A-2, B-2, and C-2 in Figs. 11(a)–11(c) were only observed between H_c and about 15 T and the signal intensity of the mode decreases with increasing magnetic fields. In IPA-$CuCl_3$, it was also reported that the intensities of two higher-lying modes observed by the INS measurements were suppressed with increasing fields,[43] which is similar to that in NDMAP. This can be caused by some similarities, i.e., 1D characteristics, between $S=1/2$ two-leg antiferromagnetic spin ladder and the $S=1$ 1D HAF.

Broadly speaking, the basic picture of the states near H_c is similar to each other between these spin-gap systems. The ground state near H_c corresponds to the dilute triplet magnons system (dilute Bose gas). The density of triplet magnons could be small and the interactions among the magnons must be negligible in the vicinity of H_c, and thus the spin excitations in these compounds show similar behavior. In the high magnetic field region ($H \gg H_c$), however, the triplet magnons are condensed and interactions among the magnons are thought to be largely different between these systems. Therefore, a change in the lifetimes of the magnon excitations, which are dependent on quantum fluctuations as described in Ref. 45, and a variation in the energy dispersion would be expected. While three dimensional weak couplings exist among dimers in $TlCuCl_3$, NDMAP has strong intrachain couplings. This difference must reflect the spin excitations and the growth of the three-dimensional correlation among magnons. The suppression of quantum fluctuations at high magnetic fields causes spin-wave-like energy states in NDMAP. Accordingly, we observed characteristic modes denoted as A-1, B-1, C-1, A-4, and B-4 in Figs. 11(a)–11(c) in the high magnetic fields and these modes are well explained by the conventional AFMR modes. Consequently, we conclude that in NDMAP, a change in the spin excitation modes from noninteractive magnon states, affected by large quantum fluctuations, to interactive magnon states is observed.

VI. CONCLUSIONS

We performed ESR measurements on single crystals of the $S=1$ quasi-1D HAF compound NDMAP in magnetic fields up to 55 T and at frequencies up to about 2 THz. First, we examined the angular dependence of spin excitation modes at the vicinity of H_c and found that two types of chains in NDMAP behave almost independently against the external magnetic field and these resonance fields are considerably explained by the PFT calculations. Disagreement between the experiment and calculation was found at high magnetic fields above 12 T.

We found that the spin excitation modes above 15 T are well explained by conventional AFMR modes with biaxial anisotropy. One of them for each principal-axis direction approaches the paramagnetic line and the other mode shows the field dependence with a gentle slope. On the other hand, between H_c and about 15 T, we observed spin excitation modes similar to those in other spin-gap systems. Accordingly, these results suggest that the spin excitations in NDMAP change from excitations by nearly noninteractive magnons, which are largely affected by quantum fluctuations, to those by interactive magnons under suppression of quantum fluctuations in high magnetic fields. Finally, we compared the results with those of the $S=1/2$ weakly coupled antiferromagnetic dimer $TlCuCl_3$ and the $S=1/2$ two-leg antiferromagnetic spin ladder IPA-$CuCl_3$ and discussed the difference in spin excitations between them above H_c.

ACKNOWLEDGMENTS

We thank A. S. Wills for his critical reading of the paper. This work was supported in part by Grants-in-Aid for Scientific Research (B) (Contract No. 20340089) and for Scientific Research on Priority Areas "High Field Spin Science in 100 T" (Contract No. 451), and by the 21st Century COE Program "Towards a New Basic Science: Depth and Synthesis" and the Global COE Program (Core Research and Engineering of Advanced Materials-Interdisciplinary Education Center for Materials Science) all from the Ministry of Education, Culture, Sports, Science, and Technology (MEXT) of Japan.

[1] *Quantum Magnetism*, Lecture Notes in Physics Vol. 645, edited by U. Schollwöck, J. Richter, D. J. J. Farnell, and R. F. Bishop (Springer, New York, 2004).
[2] F. D. M. Haldane, Phys. Lett. **93A**, 464 (1983); Phys. Rev. Lett. **50**, 1153 (1983).
[3] T. Giamarchi, *Quantum Physics in One Dimension* (Oxford University Press, New York, 2004).
[4] M. Oshikawa, M. Yamanaka, and I. Affleck, Phys. Rev. Lett. **78**, 1984 (1997).
[5] Y. Narumi, M. Hagiwara, R. Sato, K. Kindo, H. Nakano, and M. Takahashi, Physica B **246**, 509 (1998).
[6] W. Shiramura, K. Takatsu, B. Kurniawan, H. Tanaka, H. Uekusa, Y. Ohashi, K. Takizawa, H. Mitamura, and T. Goto, J. Phys. Soc. Jpn. **67**, 1548 (1998).
[7] H. Kageyama, K. Yoshimura, R. Stern, N. V. Mushnikov, K. Onizuka, M. Kato, K. Kosuge, C. P. Slichter, T. Goto, and Y. Ueda, Phys. Rev. Lett. **82**, 3168 (1999).
[8] J. G. Bednorz and K. A. Müller, Z. Phys. B: Condens. Matter **64**, 189 (1986).
[9] C. W. Chu, P. H. Hor, R. L. Meng, L. Gao, Z. J. Huang, and Y. Q. Wang, Phys. Rev. Lett. **58**, 405 (1987).
[10] H. Maeda, Y. Tanaka, M. Fukutomi, and T. Asano, Jpn. J. Appl. Phys., Part 2 **27**, L209 (1988).
[11] A. Oosawa, M. Ishii, and H. Tanaka, J. Phys.: Condens. Matter **11**, 265 (1999).
[12] T. Nikuni, M. Oshikawa, A. Oosawa, and H. Tanaka, Phys. Rev. Lett. **84**, 5868 (2000).
[13] Ch. Rüegg, N. Cavadini, A. Furrer, H.-U. Güdel, P. Vorderwisch, and H. Mutka, Appl. Phys. A: Mater. Sci. Process. **74**, S840 (2002).
[14] Ch. Rüegg, N. Cavadini, A. Furrer, H.-U. Güdel, K. Krämer, H. Mutka, A. Wildes, K. Habicht, and P. Vorderwisch, Nature (London) **423**, 62 (2003).
[15] T. Masuda, A. Zheludev, H. Manaka, L.-P. Regnault, J.-H. Chung, and Y. Qiu, Phys. Rev. Lett. **96**, 047210 (2006).
[16] N. Tateiwa, M. Hagiwara, H. A. Katori, and T. C. Kobayashi, Physica B **329B–333B**, 1209 (2003).
[17] M. Hagiwara, L.-P. Regnault, A. Zheludev, A. Stunault, N. Metoki, T. Suzuki, S. Suga, K. Kakurai, Y. Koike, P. Vorderwisch, and J.-H. Chung, Phys. Rev. Lett. **94**, 177202 (2005).
[18] L. P. Regnault, A. Zheludev, M. Hagiwara, and A. Stunault, Phys. Rev. B **73**, 174431 (2006).
[19] Z. Honda, H. Asakawa, and K. Katsumata, Phys. Rev. Lett. **81**, 2566 (1998).
[20] H. Manaka, I. Yamada, and K. Yamaguchi, J. Phys. Soc. Jpn. **66**, 564 (1997).
[21] F. H. L. Essler and I. Affleck, J. Stat. Mech.: Theory Exp. **2004**, P12006.
[22] S. Kimura, M. Hagiwara, H. Tanaka, A. K. Kolezhuk, and K. Kindo, J. Magn. Magn. Mater. **310**, 1218 (2007).
[23] M. Matsumoto, B. Normand, T. M. Rice, and M. Sigrist, Phys. Rev. Lett. **89**, 077203 (2002).
[24] M. Monfort, I. Ribas, X. Solans, and M. F. Bardia, Inorg. Chem. **35**, 7633 (1996).
[25] Figure 1 was drawn with VENUS developed by Dilanian and Izumi.
[26] Z. Honda, K. Katsumata, Y. Narumi, K. Kindo, and H. Hori, Physica B **284-288**, 1587 (2000).
[27] H. Tsujii, Z. Honda, B. Andraka, K. Katsumata, and Y. Takano, Phys. Rev. B **71**, 014426 (2005).
[28] Y. Chen, Z. Honda, A. Zheludev, C. Broholm, K. Katsumata, and S. M. Shapiro, Phys. Rev. Lett. **86**, 1618 (2001).
[29] A. Zheludev, S. M. Shapiro, Z. Honda, K. Katsumata, B. Grenier, E. Ressouche, L.-P. Regnault, Y. Chen, P. Vorderwisch, H.-J. Mikeska, and A. K. Kolezhuk, Phys. Rev. B **69**, 054414 (2004).
[30] A. Zheludev, Y. Chen, C. L. Broholm, Z. Honda, and K. Katsumata, Phys. Rev. B **63**, 104410 (2001).
[31] M. Hagiwara, Z. Honda, K. Katsumata, A. K. Kolezhuk, and H.-J. Mikeska, Phys. Rev. Lett. **91**, 177601 (2003).
[32] A. K. Kolezhuk, Phys. Rev. B **53**, 318 (1996).
[33] H. Miyazaki, T. Hiwasa, M. Oko, and I. Harada, J. Phys. Soc. Jpn. **75**, 094708 (2006).
[34] K. Kindo, Physica B **294-295**, 585 (2001).
[35] A. Zheludev, B. Grenier, E. Ressouche, L.-P. Regnault, Z. Honda, and K. Katsumata, Phys. Rev. B **71**, 104418 (2005).
[36] T. Kashiwagi, M. Hagiwara, S. Kimura, Z. Honda, and K. Kindo, J. Phys. Soc. Jpn. **76**, 103703 (2007).
[37] T. Nagamiya, K. Yoshida, and R. Kubo, Adv. Phys. **4**, 1 (1955).
[38] M. Date and M. Motokawa, J. Phys. Soc. Jpn. **22**, 165 (1967).
[39] S. Kimura, H. Ohta, and M. Motokawa, J. Phys. Soc. Jpn. **65**, 297 (1996).
[40] A. K. Kolezhuk and H.-J. Mikeska, Prog. Theor. Phys. **145**, 85 (2002).
[41] I. Affleck, Phys. Rev. B **43**, 3215 (1991).
[42] V. O. Garlea, A. Zheludev, T. Masuda, H. Manaka, L.-P. Regnault, E. Ressouche, B. Grenier, J.-H. Chung, Y. Qiu, K. Habicht, K. Kiefer, and M. Boehm, Phys. Rev. Lett. **98**, 167202 (2007).
[43] A. Zheludev, V. O. Garlea, T. Masuda, H. Manaka, L.-P. Regnault, E. Ressouche, B. Grenier, J.-H. Chung, Y. Qiu, K. Habicht, K. Kiefer, and M. Boehm, Phys. Rev. B **76**, 054450 (2007).
[44] V. N. Glazkov, A. I. Smirnov, H. Tanaka, and A. Oosawa, Phys. Rev. B **69**, 184410 (2004).
[45] I. Affleck and G. F. Wellman, Phys. Rev. B **46**, 8934 (1992).